Hindawi Publishing Corporation
Journal of Artificial Evolution and Applications
Volume 2008, Article ID 728929, 10 pages
doi:10.1155/2008/728929

Review Article

Particle Swarm Optimization for Antenna Designs in Engineering Electromagnetics

Nanbo Jin and Yahya Rahmat-Samii

Department of Electrical Engineering, University of California, Los Angeles, CA 90095-1594, USA

Correspondence should be addressed to Nanbo Jin, jnnb@ee.ucla.edu

Received 17 July 2007; Accepted 17 December 2007

Recommended by Riccardo Poli

This paper presents recent advances in applying particle swarm optimization (PSO) to antenna designs in engineering electromagnetics. By linking the PSO kernel with external electromagnetic (EM) analyzers, the algorithm has the flexibility to handle both real and binary variables, as well as multiobjective problems with more than one optimization goal. Three examples, including the designs of a dual-band patch antenna, an artificial ground plane of a surface wave antenna, and an aperiodic antenna array, are presented. Both simulation and measurement results are provided to illustrate the effectiveness of applying the swarm intelligence to design antennas with desired frequency response and radiation characteristics for practical EM applications.

1. INTRODUCTION

As access to previously unimaginable computational resources has become commonplace, many aspects of electromagnetic (EM) design have undergone titanic shifts. In particular, the fast and accurate simulation of an antenna design on a PC or parallel platforms has opened the door for stochastic optimizers to augment design processes in a large variety of engineering EM problems. As a novel evolutionary algorithm proposed in mid 1990s [1–3], particle swarm optimization (PSO) has been introduced into the EM community by one of the authors [4, 5], and its applications have received enormous attention in recent years. Unlike genetic algorithms (GAs) [6, 7], which rely on Darwin's theory of natural selection and the competition between individual chromosomes, the swarm intelligence in the nature is modelled by fundamental Newtonian mechanics in PSO for optimization purposes. This corporative scheme manifests PSO the concise formulation, the ease in implementation, and many distinct features in different types of optimizations.

In this paper, representative examples of PSO-optimized antennas developed at UCLA antenna laboratory are collected from the authors' previous publications and current research activities, in order to present the recent progress of applying swarm intelligence in practical engineering EM problems. Basic concepts in antenna design problems are introduced in Section 2, with unique advantages of applying PSO in these problems discussed. The implementation of a PSO engine for antenna optimizations is briefly described in Section 3, and three concrete design examples are presented in the following sections. The useful design guidelines provided by PSO are validated by both simulation and measurement results. The paper is summarized in Section 7.

2. ANTENNA DESIGN AS AN OPTIMIZATION PROBLEM: WHY PSO?

In transmitting or receiving systems, an antenna is a transducer of guided EM waves into propagating waves. As shown in Figure 1, the guided wave is injected into an antenna, which generates equivalent electric current $\vec{J}_{\text{eq}}$ and magnetic current $\vec{K}_{\text{eq}}$ over its enclosure. The specific configuration of antenna is not necessarily the horn as illustrated in Figure 1, and it may belong to other paradigms such as patch antennas, wire antennas, reflector antennas, or antenna arrays which assemble multiple antenna elements, and so forth. The radiation pattern of an antenna is obtained by Fourier transforming $\vec{J}_{\text{eq}}$ and $\vec{K}_{\text{eq}}$ from the spatial do-

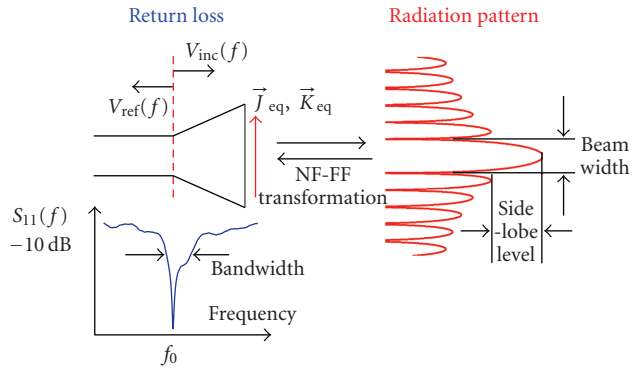

FIGURE 1: An antenna operates as a transducer of guided waves into propagating waves. The syntheses of frequency-dependent return loss and angular-dependant radiation pattern are formulated as optimization problems.

main into the angular domain. In general, the figures of merit of an antenna include the following.

Return loss

Usually the incident power is partially reflected due to the imperfect matching between the antenna and the front-end circuits. The return loss is measured by the reflection coefficient S_{11}, which is the ratio between the amplitudes of reflected wave and incident wave at the feeding point:

$$S_{11}(f) = 20\log_{10}\frac{V_{\text{inc}}(f)}{V_{\text{ref}}(f)}\,(\text{dB}), \tag{1}$$

where S_{11}, $V_{\text{inc},}$ and V_{ref} are all frequency-dependent. A standard definition of operating bandwidth is the frequency range in which $S_{11} < -10$ dB with over 90% incident power delivered to the antenna.

Radiation pattern

The radiation characteristics of an antenna, that is, the beamwidth, the sidelobe level (SLL), the directivity, and so forth, need to be synthesized to concentrate radiated power into desired directions.

Designing an antenna at a certain operating frequency f_0 (or within a bandwidth from f_L to f_H) is inherently an optimization problem. In particular, by optimizing the antenna configuration, a desired return loss can be obtained by minimizing $S_{11}(f_0)$, and a desired radiation pattern can be achieved by minimizing the difference between the actual antenna pattern and the desired pattern. The fitness functions may have different forms according to the specific application, while most antenna design problems can be categorized into these two scenarios. The evaluations of S_{11} and radiation pattern are performed by solving Maxwell equations under different boundary conditions. As a stochastic global optimizer, PSO is a good candidate to address the significant nonlinearity and multimodal effect induced by the full-wave analysis.

In antenna optimizations, the coordinates of each point in the solution space are mapped into a candidate antenna configuration. This mapping may occur from either a continuous or a discrete space to the actual design space. In many design problems, the basic antenna configuration is determined by the designer's a priori EM knowledge, while specific geometrical parameters of the antenna need to be fine-tuned to achieve the desired performance, which is a continuous optimization. In contrast, if the operating scheme of a desired antenna is relatively unknown, the design space is typically discretized into pixels and the basic antenna topology needs to be explored by optimizing a binary string to fill in the pixels. Therefore, another advantage of applying PSO to antenna designs arises from the ease and flexibility in implementing PSO for both real and binary variables. Since the only major difference between real-number and binary PSO algorithms lies in their position updating equations, real and binary variables can be even hybridized to represent a candidate design [8].

The recent popularity of PSO in antenna designs is also attributed to its capability to efficiently handle multiple design goals. In single-objective optimizations with conventional weighted aggregation (CWA), fitness functions related to different design goals are often weighted and summed. However, the weighting coefficients need to be carefully selected via trial-and-error, which is impractical for antenna optimizations that are computationally expensive. On the other hand, multiobjective PSO (MOPSO) provides an efficient way of exploiting the best tradeoff possibilities between multiple design goals. The output of MOPSO is the Pareto front that consists of a set of nondominated designs, and one has the freedom in selecting any of them according to the specific design requirement.

3. IMPLEMENTATION OF THE PSO ENGINE

With the unique advantages of applying PSO to antenna design problems discussed above, a PSO engine is implemented at UCLA with the full capability to address continuous, binary, single- and multiobjective optimizations [9]. Different EM analyzers are linked with the PSO kernel via a user-oriented interface, in order to simulate the performance of candidate antenna designs and to evaluate the fitness function. For each particular design, the user needs to select a proper optimization scenario and an EM analyzer according to the modelling of problem. A flowchart of the PSO engine is sketched in Figure 2. In this section, the implementation of different optimization scenarios is briefly described by following canonical PSO algorithms proposed in [10–12]. Optional parameters are also specified similar to the values suggested in these literature to maximize the optimizer's performance.

3.1. Real-number PSO (RPSO)

A RPSO algorithm proposed in [10] is implemented in the PSO kernel for continuous optimizations. The gbest swarm topology is used as well as in other optimization scenarios. Assume M agents are used in an N-dimensional problem,

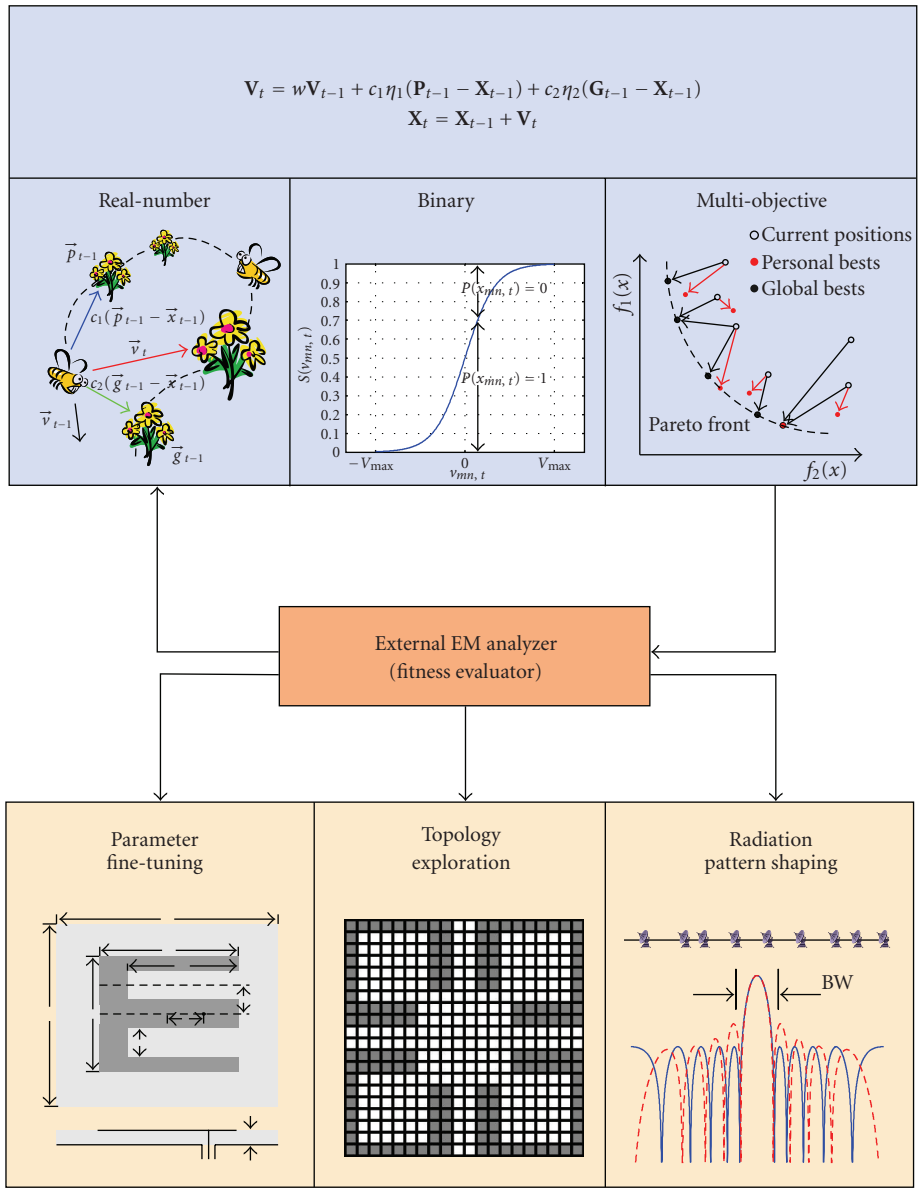

FIGURE 2: A flowchart of the PSO engine implemented at UCLA. The PSO kernel has the capability to handle continuous, binary, single- and multiobjective optimizations. Different EM analyzers are linked with the PSO kernel as external fitness evaluators.

at the tth iteration, the agents' velocities and positions are updated by

$$\mathbf{V}_t = w_t\mathbf{V}_{t-1} + c_1\eta_1 \otimes (\mathbf{P}_{t-1} - \mathbf{X}_{t-1}) + c_2\eta_2 \otimes (\mathbf{G}_{t-1} - \mathbf{X}_{t-1}), \quad (2)$$

$$\mathbf{X}_t = \mathbf{X}_{t-1} + \mathbf{V}_t. \quad (3)$$

Here, $\mathbf{V}$, $\mathbf{X}$, $\mathbf{P}$, and $\mathbf{G}$ are all $M \times N$ matrices that store the agents' velocities, positions, personal bests, and the global best, respectively. The notation $\otimes$ represents a component-wise multiplication. As suggested by [10], in the velocity updating (2), a time-varying inertia weight w_t is applied by changing its value from 0.9 at the beginning of optimization to 0.4 towards the end. Each component in matrices η_1 and η_2 has a uniform distribution in $(0, 1)$ to inject the randomness. Constants c_1 and c_2 both take a value of 2.0 to balance the cognitive and social influences.

The maximum velocity, $V_{\max}$, is imposed to prevent an agent from flying out of the physically meaningful solution space too often [13]. The value of each component of $V_{\max}$ is selected to be equal to the dynamic range of that dimension. However, this limitation does not always constrain the agent in the solution space. In [4, 14], three basic boundary handling techniques, the *absorbing* wall, the *reflecting* wall, and the *invisible* wall, are illustrated and compared. In RPSO, the invisible boundary condition is used due to its distinct advantage in reducing the computational cost.

3.2. Binary PSO (BPSO)

The BPSO subroutine in the PSO kernel follows an algorithm proposed by Kennedy and Eberhart [11]. In BPSO, the velocity update has a similar form to (2), while the agents' positions are updated via the sigmoid limiting transformation instead of directly applying (3). In particular, for the nth dimension of the mth agent, the sigmoid limiting transformation is defined as

$$S(v_{mn,t}) = \frac{1}{1 + e^{-v_{mn,t}}}, \tag{4}$$

where $v_{mn,t}$ is the agent's velocity component in the nth dimension at the tth iteration. The associated position component, $x_{mn,t}$, is updated by

$$x_{mn,t} = \begin{cases} 1, & r_{mn,t} < S(v_{mn,t}), \\ 0, & r_{mn,t} \geq S(v_{mn,t}), \end{cases} \tag{5}$$

with $r_{mn,t}$ a random number uniformly distributed in $(0, 1)$. A maximum velocity of $V_{\max} = 6.0$ is used as suggested by [11]. The inertia weight is kept as 1.0 throughout the optimization since the time varying inertia weight is observed to be harmful for the swarm's convergence in a binary solution space [9]. Boundary conditions are not necessary to be applied due to the fact that an agent will be always located in the binary solution space during the optimization.

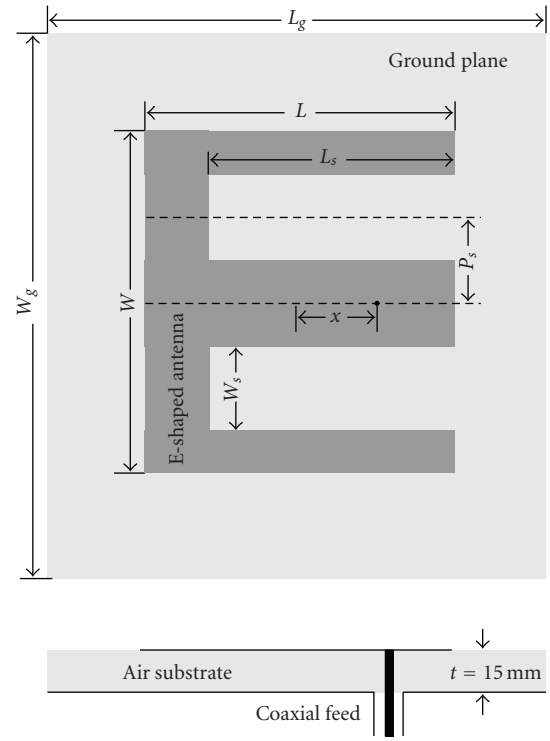

Figure 3: The topology of an E-shaped patch antenna. Each candidate design is represented by six geometrical parameters.

3.3. Multi-objective PSO (MOPSO)

Among several existing MOPSO algorithms [12, 15–17], the directed MOPSO (d-MOPSO) proposed by Fieldsend and Singh is selected due to its potential for handling more than two design objectives. In MOPSO, an archive that stores all nondominated solutions is updated at each iteration by following an algorithm proposed in [18]. The velocity and position updating equations have the same form as in single-objective PSO algorithms, while the global best of each agent is selected as the closest nondominated solution to that agent on the Pareto front in the objective space. A turbulence term is added into the velocity updating, and the magnitude of each turbulence component is one-tenth of the dynamic range of that dimension.

Before applying the PSO engine to practical antenna design problems, the algorithms described above are well examined using classic functional testbeds provided in [2] (for RPSO), [11] (for BPSO), and [15] (for MOPSO). The testing results and parameter tuning of these algorithms will not be presented here in order to keep the paper in a reasonable length, while interested readers are encouraged to refer to [14, 19] for relevant details that validate the PSO engine.

4. REAL-NUMBER PSO: A DUAL-BAND E-SHAPED PATCH ANTENNA

The first example of PSO-optimized antenna is presented in this section by applying RPSO in a parameter refinement problem [20]. In order to cover frequency bands for cellular communication systems such as the digital communication system (DCS, 1.71–1.88 GHz) and wireless local area networks (WLAN, 2.40 GH–2.48 GHz), a base station antenna is proposed in [21] for dual-band or wideband applications. The configuration of the antenna is plotted in Figure 3, which resembles a capital letter "E" and the design is therefore referred as an E-shaped antenna. Since the operating frequencies of this resonant-type antenna are closely related to current path lengths in the patch, the six geometrical parameters in Figure 3, including the patch length L, the patch width W, the slot length L_s, the slot width W_s, the slot position P_s, and the feed position x are optimized to design a dual-band antenna with resonant frequencies at 1.8 GHz and 2.4 GHz.

As discussed above, optimization of S_{11} can be formulated as a minimax problem. In other words, the relatively worse S_{11} at two desired frequencies is minimized. The fitness functions is therefore defined as

$$f = 50 + \max\{S_{11}(1.8\ \text{GHz}), S_{11}(2.4\ \text{GHz})\}. \tag{6}$$

In (6), $S_{11}(f)$ is evaluated by the finite difference time domain (FDTD) algorithm and each FDTD simulation takes about 7 minutes. The six geometrical parameters are optimized by being subjected to (unit: mm)

$$\begin{aligned} &L \in (30, 96), \quad W \in (30, 96), \quad L_s \in (0, 96), \\ &W_s \in (0, 96), \quad P_s \in (0, 96), \quad x \in (-48, 48). \end{aligned} \tag{7}$$

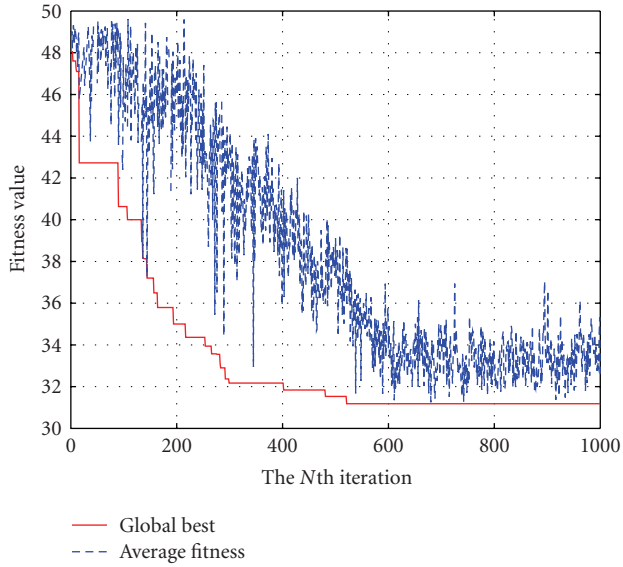

FIGURE 4: Convergence curves of the RPSO optimization by using a 10-agent swarm for 1000 iterations and applying the fitness function defined in (6).

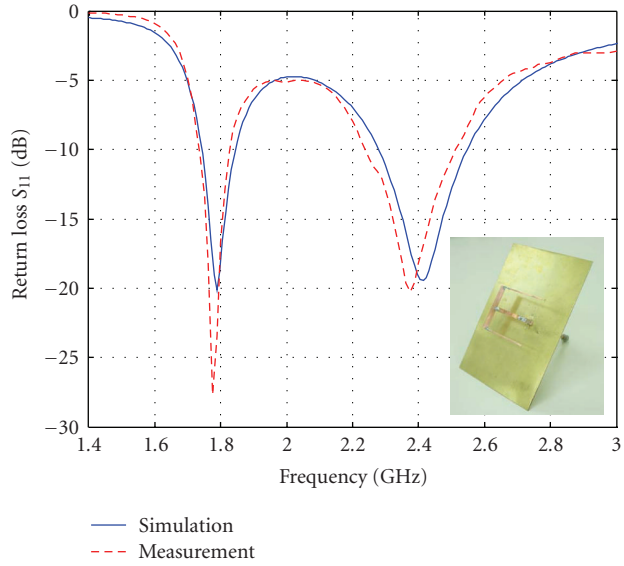

FIGURE 5: Simulated and measured S_{11} curves of the optimal dual-band antenna, which is prototyped and shown by the inset. Measurement results show a -15 dB return loss at both 1.8 GHz and 2.4 GHz.

For each candidate design, the following equations also need to be satisfied to maintain the E-shape of the patch and to retain the desired dual-band performance:

$$L_s < L, \qquad P_s > \frac{W_s}{2}, \qquad P_s + \frac{W_s}{2} < \frac{W}{2}, \qquad |x| < \frac{L}{2}. \tag{8}$$

Before evaluating the fitness function at each iteration, the six geometrical parameters are checked against (8), and the agent is treated as out-of-boundary if any equation is not satisfied.

In order to overcome the significant computational cost induced by FDTD simulations, the algorithm is implemented on 4 parallel Intel Xeon 3.0 GHz processors at UCLA Advanced Technology Service's Beowulf Linux cluster. The message passing interface (MPI) is used to communicate between the master and slave nodes. Figure 4 plots the convergence curves by using a 10-agent swarm in the optimization for 1000 iterations. The optimal design is observed after the 500th iteration with six geometrical parameters optimized as (unit: mm)

$$\begin{aligned} L &= 54.0, \quad W = 46.0, \quad L_s = 47.0, \\ W_s &= 20.0, \quad P_s = 12.0, \quad x = 14.0. \end{aligned} \tag{9}$$

The optimal dual-band antenna is prototyped and measured, with both simulated and measured S_{11} results plotted in Figure 5. A photograph of the antenna is shown by the inset. The optimal design has S_{11} values of -18.5 dB and -19.4 dB at 1.8 GHz and 2.4 GHz, respectively. The associated $S_{11} < 10$ dB bandwidths are 110 MHz at 1.8 GHz (6.1%) and 270 MHz at 2.4 GHz (11.2%). The measured results agree quite well with the simulation despite a slight frequency shift. A less than -15 dB return loss is observed at both operating frequencies.

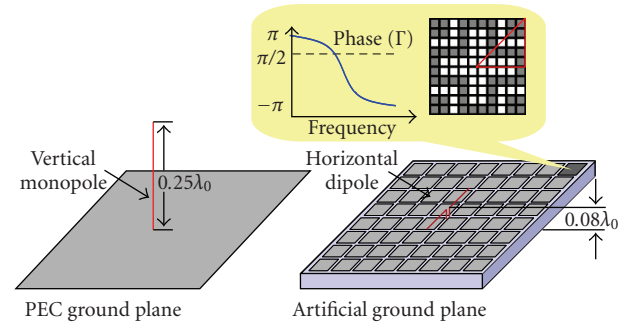

FIGURE 6: The profile of a conventional vertical dipole can be significantly reduced by an SWA. The unit cell of artificial ground plane in SWA is optimized by BPSO to match the horizontal dipole.

5. BINARY PSO: ARTIFICIAL GROUND PLANE FOR SURFACE WAVE ANTENNAS

As a comparison to the parameter refinement problem discussed above, the design of an artificial ground plane for surface wave antennas (SWAs) is presented in this section to illustrate the capability of BPSO in topology explorations. As shown in Figure 6, vertical monopole antennas with a perfect electric conductor (PEC) as the ground plane are often used in mobile communications (for instance, on the roof of a vehicle) to obtain the maximum radiation near the grazing angle. In order to reduce the profile of the antenna, which is typically a quarter free space wavelength (λ_0), a SWA is proposed in [22] by horizontally mounting a 0.28 λ_0 long dipole over an artificial ground plane.

According to the image theory in electromagnetics, it is difficult to match a horizontal dipole near the ground plane due to the radiation cancellation by the image of dipole.

However, investigations [23] have shown that by periodically loading a dielectric slab, a horizontal dipole can be well matched in a frequency band where the phase of normal reflection coefficient (Γ) of the periodic structure varies between 45° and 135°. Generally this unique reflection characteristic of periodic structure is closely related to the topology of unit cell. In this example, the unit cell with a dimension of 7.5 mm × 7.5 mm is discretized into 10 × 10 pixels. The BPSO algorithm is applied to determine the PEC/dielectric state of each pixel and explore the unit cell topology, in order to achieve the lowest center frequency of the matching band where phase (Γ) = 90°. For a fixed unit cell dimension, the optimal solution is inherently the miniaturized design that improves the homogeneity of the artificial ground plane. Compared to the optimization goal in the design of E-shaped antenna, it should be clarified that we are still trying to minimize the return loss of the SWA, while it is accomplished here in an indirect manner by characterizing the reflection coefficient of the artificial ground plane.

As shown in Figure 6, in order to achieve a polarization-independent design, the candidate unit cell has a fourfold symmetry, and only 15 pixels are optimized. A 15-bit binary string x_i ($i = 1, 2, \ldots, 15$) is used by each agent to map the candidate design into a discrete solution space. In particular, the ith pixel is filled by PEC, if $x_i = 1$, and by dielectric when $x_i = 0$. The fitness function is defined as

$$f = \text{freq}_{\text{phase}\,(\Gamma)=90^\circ} \tag{10}$$

to minimize the phase (Γ) = 90° frequency. For fabrication purpose, unit cell topologies with any two PEC pixels diagonally connected are prohibited and are assigned a very bad fitness value. The reflection phase of each candidate design is calculated by analyzing the unit cell using FDTD algorithm with periodic boundary condition, which takes about 3 minutes. In order to reduce the computational cost, an agent is checked at each iteration against the previous records before its fitness evaluation. If the same topology has been visited by the optimizer, the associated fitness value will be directly assigned to the agent with the repeated solution. The full-wave analysis is only executed for those agents located at positions that have never been explored. This repeated solution checking scheme is suitable for accelerating the BPSO process since the solution space is a finite set, particularly during the late stage of optimization when most agents have converged to the global optima.

Figure 7 plots the convergence curves by using a 10-agent swarm for 100 iterations. The global optimum is observed at the 27th iteration, and the average fitness indicates a quite good convergence at the 100th iteration. The optimal design is represented by a binary string of

$$\{x_i\} = \{000001111000111\}, \tag{11}$$

and the unit cell topology is plotted in Figure 8. The simulated reflection phase of the optimal design is also plotted. The phase (Γ) = 90° frequency is observed at 5.18 GHz.

A SWA based on the optimized artificial ground plane is fabricated and measured, as shown in Figure 9. The ground plane is etched on a 3-mm-thick substrate with a relative permittivity of 2.94 ($\epsilon_r = 2.94$) and consists of 18 × 18 optimized unit cells. Figure 10 plots measured return loss of the SWA. The antenna has a minimum return loss of 5.26 GHz, which is only 1.5% off the optimized phase (Γ) = 90° frequency at 5.18 GHz. Also plotted in Figure 10 is the S_{11} curve of a horizontal dipole with the same size on a PEC ground plane. It is observed that the matching of antenna is significantly deteriorated due to the existence of image dipole. The measured radiation pattern of SWA is shown in Figure 11, where maximum radiations are observed at 70° and 290°. Compared to the pattern of a vertical monopole on a PEC ground plane with the same size of $2.4\lambda_0 \times 2.4\lambda_0$, the pattern

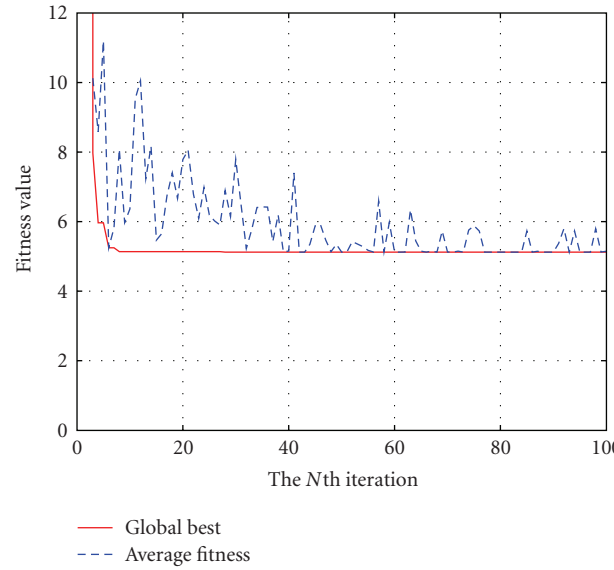

Figure 7: Convergence curves of the BPSO optimization by using 10 agents for 100 iterations. The fitness function is defined in (10).

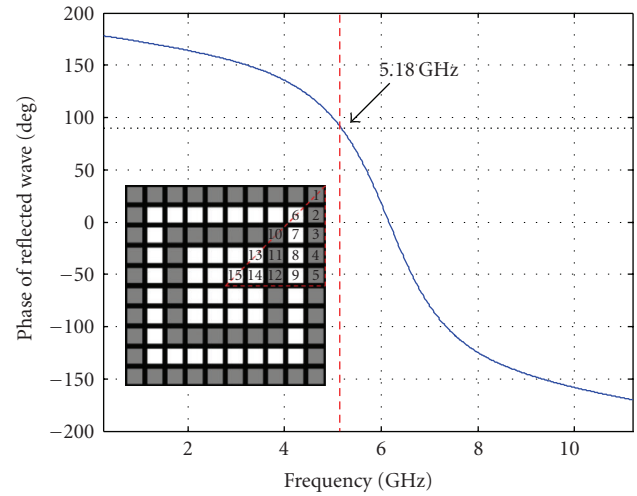

Figure 8: Simulated reflection phase of the optimal design with a phase (Γ) = 90° frequency of 5.18 GHz observed. The optimal unit cell topology is plotted by the inset.

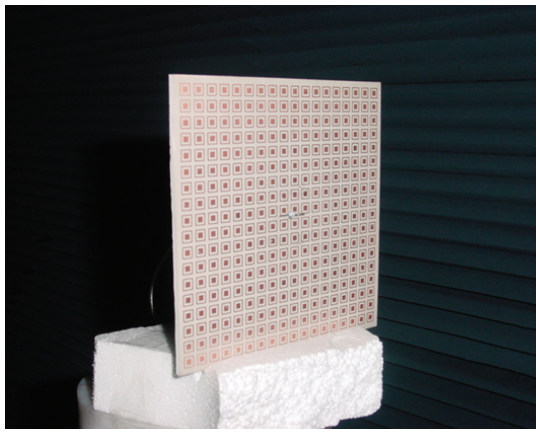

Figure 9: An SWA is fabricated based on the artificial ground plane which consists of 18×18 optimized unit cells.

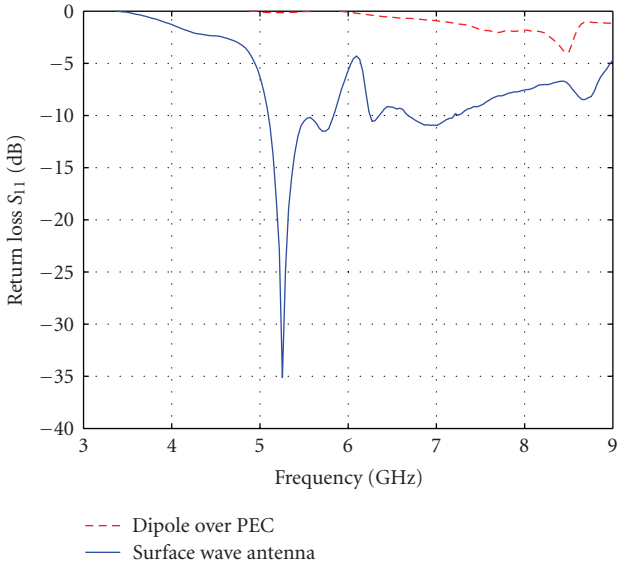

Figure 10: Measured S_{11} of the SWA. Compared to a horizontal dipole over a conventional PEC ground, the SWA is well matched at 5.26 GHz with a return loss of −35 dB.

of SWA shows a great similarity, while the 0.25 λ_0-profile of the vertical monopole is reduced to 0.08 λ_0 in this example.

6. MULTIOBJECTIVE PSO: LOW-SIDELOBE APERIODIC ANTENNA ARRAYS

Antenna arrays have been broadly used in communication and radar systems where a highly directive radiation pattern is desired. For conventional periodic arrays, complete design and synthesis theories have been established for several decades. However, grating lobes (sidelobes with the same level as the main beam) in the radiation patterns of periodic arrays are inevitable, when the uniform element spacing is greater than λ_0. In recent years, evolutionary algorithms have been extensively used in the design of aperiodic antenna arrays to obtain the lowest peak SLL [24–27]. In this example, MOPSO is applied to design an 8-element nonuniform

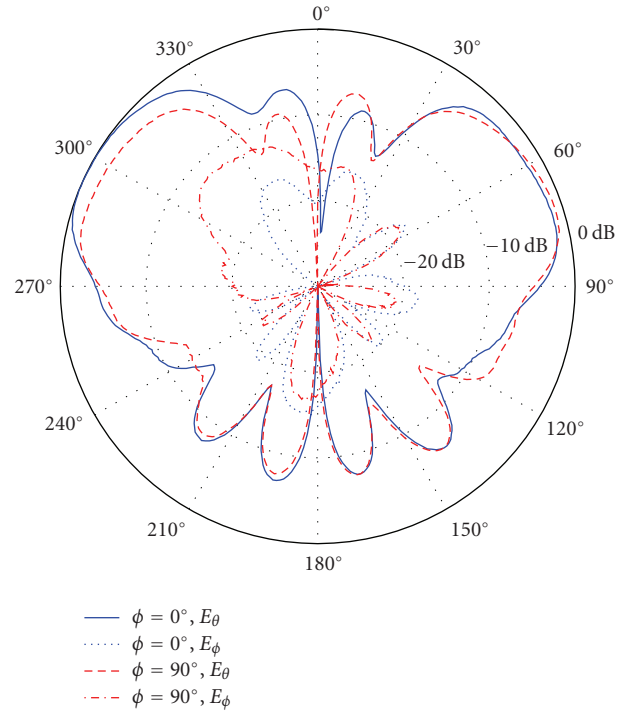

Figure 11: Measured radiation pattern of the SWA which resembles the pattern of a vertical monopole.

antenna array by optimizing the element positions, in order to investigate the best tradeoff between its peak SLL and beamwidth.

An 8-element linear nonuniform array is shown in Figure 12. The antenna elements are identical patch antennas etched on an 0.787 mm thick substrate with $\epsilon_r = 2.2$. The dimension of each patch antenna is $0.49\lambda_g \times 0.70\lambda_g$ $(0.33\lambda_0 \times 0.48\lambda_0)$. The array is assumed to be symmetric with respect to the z-axis, and the array configuration is mapped into a 4-dimensional real-valued solution space $\{d_i\}$ $(i = 1, 2, 3, 4)$ which represents the element spacings. All elements are allowed to vary within $\pm 5.0\lambda_0$, which gives a maximum element spacing of $d_{\text{avg}} = 1.43\lambda_0$. To prevent adjacent elements from getting overlapped, the element spacings are subjected to

$$d_1 \in (0.24\lambda_0, 3.56\lambda_0), \qquad d_2, d_3, d_4 \in (0.48\lambda_0, 3.8\lambda_0),$$
$$\sum_{i=1}^{4} d_i \le 5.0\lambda_0. \tag{12}$$

The lower bound of each variable is defined according to the width of patch, and the upper bound is calculated by assuming that other three patches are connected to each other.

The peak SLL and the null-to-null beamwidth are represented by the following two fitness functions:

$$f_1 = \max\{20\log|\text{AF}(\theta) \times \text{EF}(\theta)|\}, \quad 0° < \theta < \theta_n,$$
$$f_2 = 2(90^\circ - \theta_n), \tag{13}$$

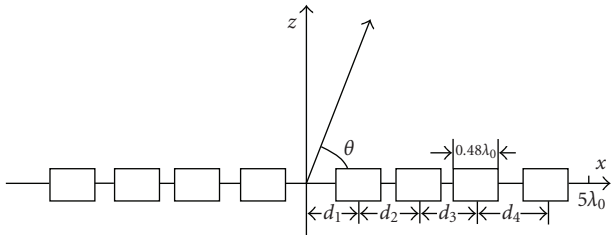

Figure 12: An 8-element, symmetric, nonuniform antenna array with a maximum aperture size of 10 λ_0. The element positions are optimized by MOPSO to investigate the best tradeoff relationship between its peak SLL and beamwidth.

where AF(θ) and EF(θ) are the array factor, and the element pattern analytically calculated by

$$\mathrm{AF}(\theta) = \sum_{i=1}^{4} \cos\left[2\pi \sum_{k=1}^{i} d_k(\cos\theta)\right], \tag{14}$$

$$\mathrm{EF}(\theta) = \tan\theta \sin(0.49\cos\theta), \tag{15}$$

respectively. θ_n denotes the position of the first null away from the broadside ($\theta = 90^\circ$). It should be noted that the radiation pattern only depends on the elevation angle θ in this linear array case. Compare to the general pattern optimization problem discussed in Section 2, the fitness function has a simpler form since the design goal is to achieve the minimum peak SLL instead of matching a desired pattern in the entire angular domain.

The optimization is executed for 4000 iterations using a 20-agent swarm. Figure 13 plots the Pareto front. Each nondominated design located at (ξ, η) can be interpreted as, for any design that has a null-to-null beamwidth of η-degree, its peak SLL can not be lower than ξ-dB. As a comparison, the beamwidth-SLL relationship of an 8-element periodic array is plotted in Figure 13. This curve is completely dominated by the Pareto front, which indicates that an aperiodic array on the Pareto front always has a lower SLL than a periodic array with the same beamwidth. For instance, design A is arbitrarily selected from the Pareto front with optimized element spacings of

$$\{d_i\} = \{0.49\lambda_0,\ 2.17\lambda_0,\ 1.13\lambda_0,\ 1.21\lambda_0\}, \tag{16}$$

and an aperture size of 10 λ_0. Compared to a periodic array with the same aperture size, A', the aperiodic array has a similar beamwidth but a significantly reduced peak SLL. Their radiation patterns calculated by (14) and (15) are plotted in Figure 14. The periodic array A' has a high SLL of -4.3 dB due to the strong grating lobes in the array factor, while design A has a much lower SLL of -10.1 dB by aperiodically arranging the elements and eliminating the grating lobes. The directivities of arrays A' and A are 17.2 dB and 17.6 dB, respectively.

Figure 15 shows fabricated prototypes of both arrays, and their measured radiation patterns at the operating frequency of 15 GHz are shown in Figure 16. It is observed that the -3.9 dB grating lobes of the periodic array are reduced

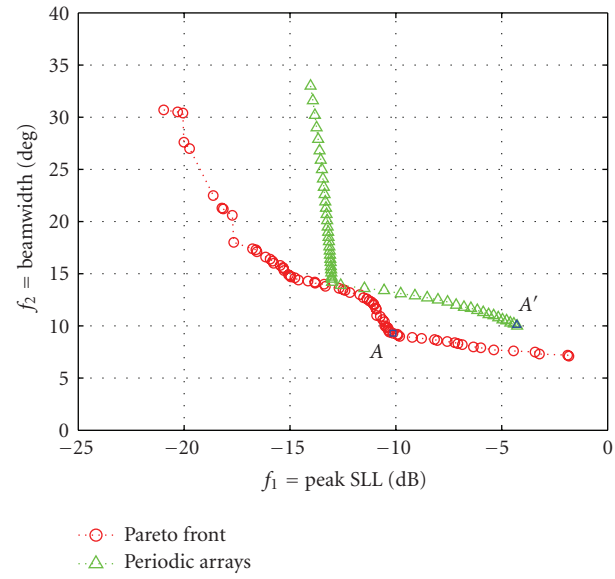

Figure 13: The Pareto front of the MOPSO optimization for trading off the peak SLL and the beamwidth of an 8-element nonuniform patch antenna array. The SLL-beamwidth relationship of periodic arrays is also plotted.

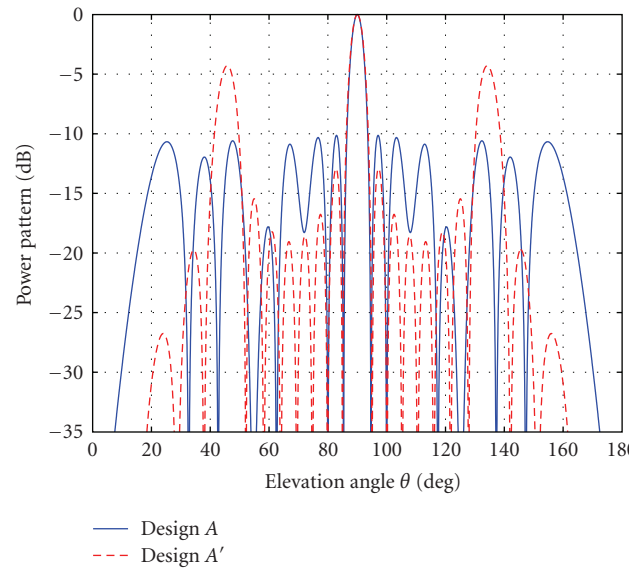

Figure 14: Comparison between the radiation patterns of a selected nonuniform array A and a periodic array A' in Figure 13.

to -9.6 dB, and the nonuniform array exhibits an approximate equal-sidelobe feature. Furthermore, the beamwidth, the number, and the location of sidelobes of both arrays agree fairly well with the analytical simulation results shown in Figure 14. It is believed that in the fabricated antenna arrays, the mutual coupling is considerably small due to a large $d_{\mathrm{avg}} = 1.43\lambda_0$, which makes the optimization result a good prediction for designing a low-SLL array with a sparse configuration.

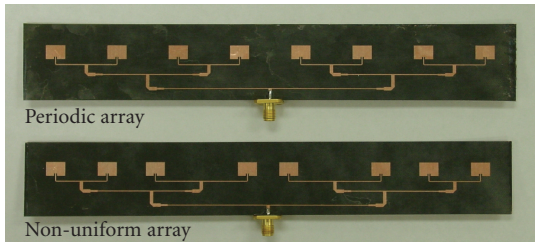

Figure 15: Fabricated array prototypes of designs A and A' in Figure 13.

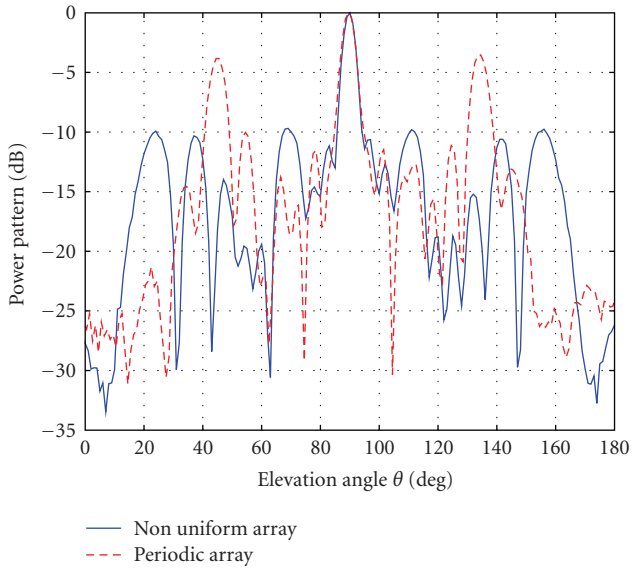

Figure 16: Measured radiation patterns of designs A and A'. Grating lobes of the periodic array are eliminated by the nonuniform array configuration.

7. CONCLUSION

The enormous interest in applying PSO technique to antenna designs is evident due to the wide range of practical problems that can be solved by this novel, nature-inspired, evolutionary algorithm. Modelled by fundamental Newtonian mechanics, the swarm intelligence is imbedded in the design process to accommodate different types of optimizations. With this powerful PSO engine available, it is relatively easy to apply it to different problems without making significant changes to the kernel of the optimizer.

In this paper, we only present three examples to illustrate the functionality of PSO in a large variety of real-world problems. These examples are categorized into the optimizations of return loss and radiation pattern, while the flexibility in defining the fitness function allows PSO to address other design requirements. It is observed that as a stochastic global optimizer, PSO is particularly suitable for antenna optimizations which are in general extremely nonlinear and multimodal. Both simulation and measurement results of PSO-optimized antennas are presented in each example, in order to validate the capability of PSO in producing a useful and practical design.

REFERENCES

[1] J. Kennedy and R. Eberhart, "Particle swarm optimization," in *Proceedings of IEEE International Conference on Neural Networks*, vol. 4, pp. 1942–1948, Perth, Wash, Australia, 1995 November.

[2] J. Kennedy and R. Eberhart, *Swarm Intelligence*, Morgan Kaufmann, San Francisco, Calif, USA, 2001.

[3] R. Poli, J. Kennedy, and T. Blackwell, "Paticle swarm optimization: an overview," *Swarm Intelligence*, vol. 1, no. 1, pp. 33–57, 2007.

[4] J. Robinson and Y. Rahmat-Samii, "Particle swarm optimization in electromagnetics," *IEEE Transactions on Antennas and Propagation*, vol. 52, no. 2, pp. 397–407, 2004.

[5] Y. Rahmat-Samii, D. Gies, and J. Robinson, "Particle swarm optimization (PSO): a novel paradigm for antenna designs," *The Radio Science Bulletin*, vol. 305, pp. 14–22, 2003.

[6] D. Goldberg, *Genetic Algorithms in Search, Optimization and Machine Learning*, Addison-Wesley, Reading, Mass, USA, 1989.

[7] Y. Rahmat-Samii and E. Michielssen, Eds., *Electromagnetic Optimization by Genetic Algorithms*, John Wiley & Sons, New York, NY, USA, 1999.

[8] N. Jin and Y. Rahmat-Samii, "A hybrid real-binary particle swarm optimization (HPSO) algorithm: concepts and implementations," in *Proceedings of IEEE Antennas Propagation International Symposium*, pp. 1585–1588, Honolulu, Hawaii, USA, 2007 June.

[9] N. Jin and Y. Rahmat-Samii, "Advances in particle swarm optimization for antenna designs: real-number, binary, single-objective and multiobjective implementations," *IEEE Transactions on Antennas and Propagation*, vol. 55, no. 3 I, pp. 556–567, 2007.

[10] Y. Shi and R. Eberhart, "Empirical study of particle swarm optimization," in *Proceedings of the IEEE Congress on Evolutionary Computation (CEC '99)*, vol. 3, pp. 1945–1950, Washington, DC, USA, 1999 July.

[11] J. Kennedy and R. Eberhart, "A discrete binary version of the particle swarm algorithm," in *Proceedings of IEEE International Conference on Systems, Man, and Cybernetics (SMC '97)*, vol. 5, pp. 4104–4108, Orlando, FLa, USA, 1997 October.

[12] J. Fieldsend and S. Singh, "A multi-objective algorithm based upon particle swarm optimisation, an efficient data structure and turbulence," in *Proceedings of the U.K. Workshop on Computational Intelligence (UKCI '02)*, pp. 37–44, Birmingham, UK, 2002 September.

[13] R. Eberhart and Y. Shi, "Comparing inertia weights and constriction factors in particle swarm optimization," in *Proceedings of IEEE Congress on Evolutionary Computation (CEC '00)*, vol. 1, pp. 84–88, La Jolla, Calif, USA, 2000 July.

[14] S. Xu and Y. Rahmat-Samii, "Boundary conditions in particle swarm optimization revisited," *IEEE Transactions on Antennas and Propagation*, vol. 55, no. 3 I, pp. 760–765, 2007.

[15] K. E. Parsopoulos and M. N. Vrahatis, "Recent approaches to global optimization problems through particle swarm optimization," *Natural Computing*, vol. 1, no. 2-3, pp. 235–306, 2002.

[16] X. Hu and R. Eberhart, "Multiobjective optimization using dynamic neighborhood particle swarm optimization," in *Proceedings of IEEE Congress on Evolutionary Computation (CEC*

'02), vol. 2, pp. 1677–1681, Honolulu, Hawaii, USA, 2002 May.

[17] C. Coello Coello and M. Lechuga, "MOPSO: a proposal for multiple objective particle swarm optimization," in *Proceedings of IEEE Congress on Evolutionary Computation (CEC '02)*, vol. 2, pp. 1051–1056, Honolulu, Hawaii, USA, 2002 May.

[18] Y. Jin, M. Olhofer, and B. Sendhoff, "Dynamic weighted aggregation for evolutionary multiobjective optimization: why does it work and how?" in *Proceedings of the Genetic and Evolutionary Computation Conference (GECCO '01)*, pp. 1042–1049, San Francisco, Calif, USA, 2001 July.

[19] D. Gies, "Particle swarm optimization: applications in electromagnetic design," M. Eng. thesis, Los Angeles, Calif, USA, 2004.

[20] N. Jin and Y. Rahmat-Samii, "Parallel particle swarm optimization and finite difference time-domain (PSO/FDTD) algorithm for multiband and wide-band patch antenna designs," *IEEE Transactions on Antennas and Propagation*, vol. 53, no. 11, pp. 3459–3468, 2005.

[21] F. Yang, X.-X. Zhang, X. Ye, and Y. Rahmat-Samii, "Wide-band E-shaped patch antennas for wireless communications," *IEEE Transactions on Antennas and Propagation*, vol. 49, no. 7, pp. 1094–1100, 2001.

[22] F. Yang and Y. Rahmat-Samii, "Wire antennas on artificial complex ground planes: a new generation of low gain antennas," in *Proceedings of IEEE Antennas Propagation International Symposium*, vol. 1, pp. 309–312, Monterey, Calif, USA, 2004 June.

[23] F. Yang and Y. Rahmat-Samii, "Reflection phase characterizations of the EBG ground plane for low profile wire antenna applications," *IEEE Transactions on Antennas and Propagation*, vol. 51, no. 10, pp. 2691–2703, 2003.

[24] R. Haupt, "Thinned arrays using genetic algorithms," in *Electromagnetic Optimization by Genetic Algorithms*, Y. Rahmat-Samii and E. Michielssen, Eds., John Wiley & Sons, New York, NY, USA, 1999.

[25] K. Chellapilla, S. S. Rao, and A. Hoorfar, "Optimization of thinned phased arrays using evolutionary programming," in *Proceedings of the 7th International Conference on Evolutionary Programming*, vol. 1447, pp. 157–166, San Diego, Calif, USA, 1998 March.

[26] D. Gies and Y. Rahmat-Samii, "Particle swarm optimization for reconfigurable phase-differentiated array design," *Microwave and Optical Technology Letters*, vol. 38, no. 3, pp. 172–175, 2003.

[27] D. W. Boeringer and D. H. Werner, "Particle swarm optimization versus genetic algorithms for phased array synthesis," *IEEE Transactions on Antennas and Propagation*, vol. 52, no. 3, pp. 771–779, 2004.